Soft Matter

Dynamic Article Links

Cite this: *Soft Matter*, 2012, **8**, 5250

www.rsc.org/softmatter

PAPER

Internal microstructures in shearing giant electrorheological fluids

Cong Li,[a] Junying Huang,[a] Qiangguo Tang,[a] Jiping Huang,*[a] Jianwei Zhang[b] and Luwei Zhou*[a]

Received 23rd February 2012, Accepted 2nd March 2012
DOI: 10.1039/c2sm25424g

The macroscopic physical properties of giant electrorheological (GER) fluids are crucially dependent on their internal particle microstructure. However, GER fluids are often sheared in work, which makes it difficult to clearly observe their internal microstructure *via* existing experimental tools. Here, an experimental method has been developed to observe the lamellar microstructures of GER fluids, which fill the space between two relatively rotating parallel disk electrodes (disk–disk geometry). Nevertheless, only microstructures in surface regions can be observed in the shearing process *via* some experimental approaches. We incorporated two fluid phase models of ER fluids and the mechanism of GER fluids in order to study the GER fluids in the shearing process. Internal microstructures of GER fluids shearing in the whole region simultaneously were discovered for the first time. The internal system produces a variety of complex patterns and dynamics. The patterns are caused by the fluctuation frequency of radial shear bands; and there exist vertical shear bands which give rise to delamination perpendicular to the flow direction. The distribution of radial and vertical shear bands in the inner geometry is governed by the Onsager principle of minimum energy dissipation rate.

1 Introduction

The macroscopic physical properties of electrorheological (ER) or giant ER (GER) fluids are crucially dependent on their internal particle microstructures.[1–7] Under an electric field, ER/GER particles tend to aggregate and form chains/columns along the direction of the field. In this process, there exists a competition mainly between the electrostatic energy and the entropy of the particles, and finally the system reaches a solid-like state. The static yield stress of GER fluids is about ten to a hundred times larger than that of ER fluids. Furthermore, a prominent feature of GER fluids is the near-linear dependence of the yield stress on the electric field, in contrast to the quadratic variation usually observed in ER fluids.[2,8] GER fluids in most applications are often under shear stress,[9,10] where the static chain/column structures no longer exist. Henley and Filisko observed that only ER fluids with strong ER activity possess lamellar microstructures perpendicular to the electric field direction.[1] The lamellar microstructure phenomenon is caused by concentration fluctuation under shear flow. However, it is difficult to observe the three-dimensional flow profiles of a dense shearing GER fluid because traditional optical methods are limited by the large refractive index mismatch between the particles and the oil. In this work, we experimentally observed the surface lamellar microstructures of shearing GER fluids confined in the space between two relatively rotating parallel disk electrodes (disk–disk geometry); further simulations were performed to study the internal microstructures using the two phase fluid models.[11–13] Both results show that internal lamellar microstructures and shear bands, which are dominated by the Onsager principle of minimum energy dissipation rate, exist in the disk–disk geometry. Thus, one must take into account the shearing effect of GER fluids in real applications.

2 Experiments

The GER fluid used in this study is a mixture of silicone oil and TiO_2 particles coated with 1,4-butyrolactone. The particles are prepared from amorphous TiO_2 by the sol–gel method.[14] The powder with an average diameter of 919.4 nm shows an irregular morphology. Our previous work[14] shows that this fluid has the properties of a GER fluid when the electric field is turned on: the static yield stress of GER fluids is about ten to a hundred times larger than that of dielectric (conventional) ER fluids; there is a near-linear dependence of the yield stress on the electric field, in contrast to the quadratic variation usually observed in ER fluids. The volume fraction of the GER fluid is 35%. An electrorheoscope[7] is an electrorheometer with an attached microscope. Two such electrorheoscopes are made to respectively record top and bottom views of structure change of ER fluids while simultaneously measuring their electrorheological properties. The bottom viewed electrorheoscope is established from a Haake-Mars II electrorheometer by attaching it with a microscope and a CCD video adaptor. The top electrode rotates, and the bottom

[a]*State Key Laboratory of Surface Physics and Department of Physics, Fudan University, Shanghai 200433, China. E-mail: jphuang@fudan.edu.cn; lwzhou@fudan.edu.cn*
[b]*Shanghai Key Laboratory of Special Artificial Microstructure Materials and Technology and Department of Physics, Tongji University, Shanghai 200092, China*

transparent one is static. In this way, a bottom view of the lamellar microstructure can be recorded through the bottom transparent electrode. The DC electric field is perpendicular to the electrodes in both electrorheoscopes. The experimental disk–disk geometry, which is identical to our simulation geometry, is shown in Fig. 1 (a). The outer radius of the two plates is 17.5 mm and the gap between them is 1 mm. Fig. 1 (b) shows the axially symmetric profile of the disk–disk geometry.

Fig. 2 shows the experimental results of surface lamellar microstructures for six different conditions. The dark and light regions represent the high and low particle concentrations, respectively. h represents the distance to the bottom electrode. Fig. 2 (a^{top})–(f^{top}) show the top views of lamellar microstructures (h = 1.0 mm) which are taken using the home-made electrorheoscope. Fig. 2 (a^{bottom})–(f^{bottom}) show the bottom views of the lamellar microstructures (h = 0.0 mm), which are taken using the electrorheoscope modified from the Haake-Mars II electrorheometer. The higher the electric field and the lower the shear rate, the more GER particle rings appear. This property of forming lamellar microstructures is also found in GER fluids, and it is similar to traditional ER fluids.[15] To our surprise, the top and bottom views of the lamellar microstructures are quite different under the same electric field and shear flow. But it is difficult to experimentally observe the three-dimensional internal microstructures of the entire system simultaneously because of the opacity of the GER fluids. In the following section, we determine the internal lamellar microstructures by means of computer simulations.

3 Computer simulations

The Onsager principle of minimum energy dissipation is about the rules governing the optimal paths of deviation from and restoration to equilibrium.[11,16–19] It provides great flexibility in choosing state variables, and thus is quite convenient for solving problems involving non-equilibrium systems. The Navier–Stokes equations of motion for fluids and ER particles are deduced from the Onsager principle of minimum energy dissipation.[11,18,19] In this study, we extend this principle to a GER fluid confined in the disk–disk geometry, using saturated orientation polarization

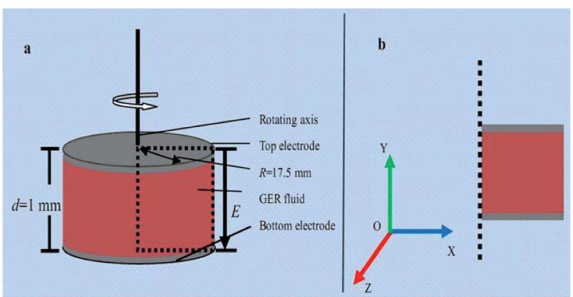

Fig. 1 (a) Schematic of the experimental disk–disk geometry. The GER fluid fills the gap between the two parallel transparent disks (when one disk is rotating and the other is static). (b) Axially symmetric profile of the disk–disk geometry. For convenience, a sample rectangle cell is established in two-dimensional axially symmetric coordinates. The symmetric axis is the rotating axis and parallel to the electric field, E. The direction of shear flow is along $-Z$ axis.

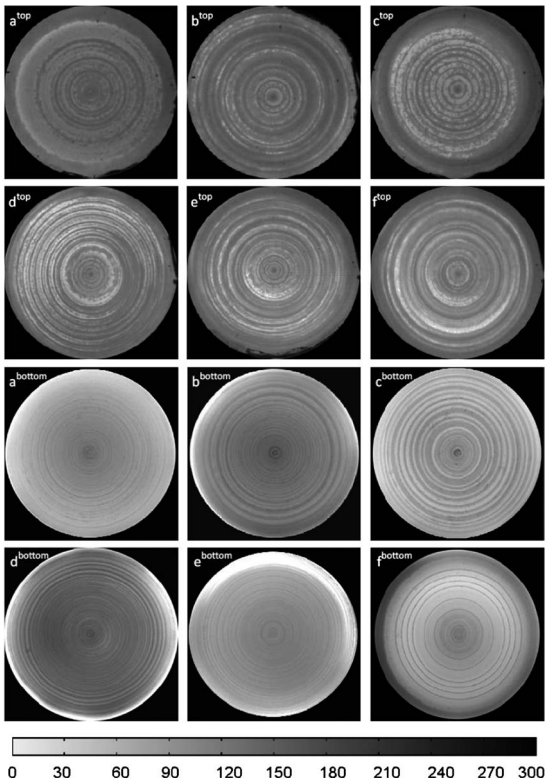

Fig. 2 Experimental results: Top and bottom surface lamellar microstructures of the GER fluid in the disk–disk geometry for different values of shear rate and electric field. The degree of shading represents the relative concentration of the particles. Panels (a^{top})–(f^{top}) show the top views of the lamellar microstructures (h = 1 mm, h represents the distance to the bottom electrode) measured with the home-made electrorheometer: panels (a^{top}), (b^{top}) and (c^{top}) are at the same shear rate of $\dot{\gamma}$ = 549.5 s^{-1}, and are under E = 0.5, 0.9 and 1.3 kV mm^{-1}, respectively; panels (d^{top}), (e^{top}) and (f^{top}) are under the same electric field of E = 1.1 kV mm^{-1}, and are at $\dot{\gamma}$ = 641.1, 1007.4 and 1373.8 s^{-1}, respectively. Panels (a^{bottom})–(f^{bottom}) are the corresponding bottom viewed lamellar microstructures (h = 0 mm) taken with a Haake-Mars II electrorheometer.

theory.[2,20] The maximum local electric field between two closely contacting GER particles is[21]

$$E_{local} = E_l + L_\alpha(E_{local})\frac{nu}{\varepsilon_f} \quad (1)$$

where $E_l = \beta E_0$ is estimated from the finite element analysis. Here β denotes a local-field enhancement factor determined by the dielectric properties of GER fluids. The orientational probability of polar molecules, $L_\alpha(E) = (e^\alpha + e^{-\alpha})/(e^\alpha - e^{-\alpha}) - 1/\alpha$ with $\alpha = uE/kT$, where u is the permanent dipole moment of a polar molecule, k is the Boltzmann constant, and T is the absolute temperature. Then, the effective dipole moment of the polar molecules located in the outer shell of a GER particle is $p = nuL_\alpha(E)$ where n is the number density of polar molecules. The chemical potential is

$$\mu[n'(\vec{x})] = -\vec{E}_{local}(\vec{x})\cdot\vec{p}(\vec{x}) + \varepsilon_0\int\left(\frac{a}{|\vec{x}-\vec{y}|}\right)^{12} n'(\vec{y})\,d\vec{x} \quad (2)$$

where the first term on the right is the potential of the GER particles at $\vec{x}$ caused by the local electric field. The second term is

the repulsive interaction potential between a particle at $\vec{x}$ and its neighbours at $\vec{y}$. The force density is $n'\nabla\mu$. n' is the number density of GER particle rings. We next introduce the GER force density into the two phase dipole fluid model:[11,18,19]

$$\rho_p\left(\frac{\partial \vec{V}_p}{\partial t}+\vec{V}_p\cdot\nabla\vec{V}_p\right)=-\nabla p_p+\nabla\cdot\tau^p_{visc}+n'\nabla\mu+K\left(\vec{V}_f-\vec{V}_p\right) \tag{3}$$

$$\rho_f\left(\frac{\partial \vec{V}_f}{\partial t}+\vec{V}_f\cdot\nabla\vec{V}_f\right)=-\nabla p_f+\nabla\cdot\tau^f_{visc}+K\left(\vec{V}_p-\vec{V}_f\right) \tag{4}$$

$$\dot{n}'+\vec{\nabla}\cdot\vec{J}=\partial_t n+\vec{V}_p\cdot\vec{\nabla}n'+\vec{\nabla}\cdot\vec{J}=0 \tag{5}$$

Eqn. 3 is the Navier–Stokes equation of motion for the particle phase ("p"); eqn. 4 is for the fluid ("f") phases; eqn. 5 is the continuity equation. ρ_p is the local mass density of the particle phase, and ρ_f is the local mass density of the fluid phase. $\vec{V}_p$ and $\vec{V}_f$ are the velocities for the particle and the fluid phases, respectively; p_p and p_f are the pressures in the solid and liquid phases, respectively; τ^p_{visc} and τ^f_{visc} are the viscous stress of the particle phase and the fluid phase, respectively. $\vec{J}$ is a convective–diffusive current density.

To simulate the region between the two rotating electrodes, a sample cell of thickness 1 mm and length 17.5 mm is established in a two-dimensional axially symmetric coordinate. The rotating axis is along the short side of the cell and parallel to the electric field as shown in Fig. 1 (b). This area is later referred to as the "axial symmetric profile". The upper long side lies on the upper rotating electrode which causes the GER fluid to circulate. In this study, solid particles are considered to be spherical with diameter 919.4 nm, dielectric constant $\varepsilon_p = 38$ and mass $m = 1.2 \times 10^{-15}$ kg. The mass density of the particles is 1.79 g cm^{-3}. Particles are suspended in oil with dielectric constant $\varepsilon_f = 2.5$, dynamic viscosity $\eta_f = 0.01$ Pa s and mass density $\rho_f = 0.96$ g cm^{-3}. Due to the joint effects of thermal fluctuation and viscous forces, the mass density difference between the oil and the particles can be used to avoid significant sedimentation of the particles during the experiments. In this work we do not consider the interfacial energy. The volume fraction of the GER particles is 35%. To model realistic systems, we added a slip length of 10 μm at the boundary for both particle and oil phases. We implemented the simulation by utilizing the finite element approach, based on the commercial software COMSOL Multiphysics 3.5a.

4 Results and discussion

4.1 Comparison between experiments and computer simulations

Using the exact same values for the shear rate and electric field as in experiments, lamellar microstructures of the GER fluid in the disk–disk geometry are simulated using the Onsager principle. Under $\dot{\gamma} = 549.5$ s^{-1}, and $E = 1.3$ kV mm^{-1} the viscosity is 2.85 Pa s, and when the electric field is turned off the viscosity comes to 0.012 Pa s. As shown in Fig. 3, the higher the electric-field strength and the lower the shear rate the more GER particle rings appear in the pattern; there also exists a difference between top and bottom lamellar microstructures as in experiments. We calculated the number density of particle rings using

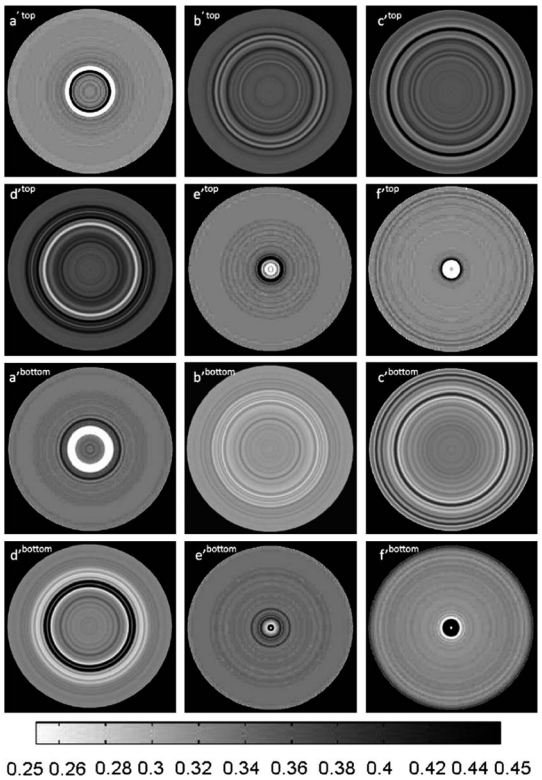

Fig. 3 Computer simulation results: Top and bottom surface lamellar microstructures of the GER fluid between two relatively rotating parallel disk electrodes under the same electric field and rotating speed conditions as in the experiments. The degree of shading represents particle concentration. Panels (a′^{top})–(f′^{top}) show the top view of lamellar microstructures (h = 1 mm): (a′^{top}), (b′^{top}) and (c′^{top}) are at the same shear rate of $\dot{\gamma} = 549.5\ s^{-1}$, with electric fields of $E = 0.5$, 0.9 and 1.3 kV mm^{-1}, respectively; (d′^{top}), (e′^{top}) and (f′^{top}) are under the same electric field of $E = 1.1$ kV mm^{-1}, with shear rates of $\dot{\gamma} = 641.1$,1007.4 and 1373.8 s^{-1} respectively. Panels (a′^{bottom})–(f′^{bottom}) show the corresponding bottom viewed lamellar microstructures (h = 0 mm).

$n_r = N/(\pi R^2)$, where N is the number of particle rings, and R = 17.5 mm. The number densities of particle rings on each surface shown in Fig. 2 and Fig. 3 are displayed in Fig. 4. The trend for n_r obtained from our simulations is consistent with our experimental results. Square and triangle symbols represent experimental results (Fig. 2) and computer simulation results (Fig. 3), respectively. Solid symbols and hollow symbols represent top and bottom views, respectively. The same conclusion holds, namely that the higher the electric-field strength and the lower the shear rate, the more particle rings appear, which means that our theoretical model is suitable for understanding dynamic GER effects. The advantage of computer simulation is its representation of not only the bulky three-dimensional (3D) lamellar microstructures, but also the profile of particle tangential velocities.

4.2 Internal microstructures with computer simulations

The internal microstructure is very important in the study of the macroscopic physical properties of shearing GER fluids. To challenge this, we calculated the transient internal lamellar

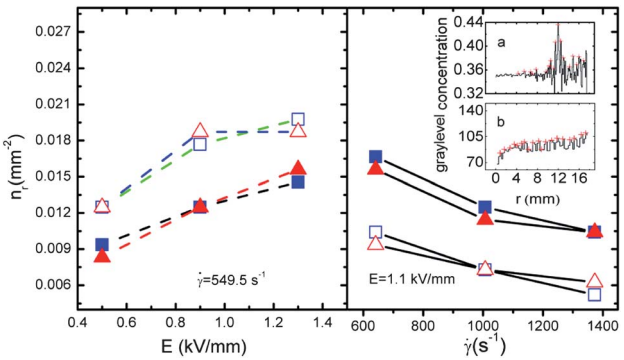

Fig. 4 (Color online) A comparison of particle ring densities between experiments and computer simulation. Square and triangle symbols represent experimental results (Fig. 2) and computer simulation results (Fig. 3), respectively. Solid and hollow symbols represent top and bottom views, respectively. In the insets, the red plus signs obtained using Origin indicate the position of particle rings; a is for simulation and b is for experiments.

microstructures at different heights, h, from the bottom static electrode (or along the Y-axis as shown in Fig.1 (b)). There exist rich internal 3D lamellar microstructures with different patterns as shown in Fig.5 (a). It looks as though the degree of shading for panels of $h = 1.0$ and 0.0 mm is higher than that for other panels. Due to the non-equilibrium electric force close to the electrodes, the dielectric particles aggregate at the top and bottom electrodes. This demonstrates that there is an obvious weakening of the internal microstructure of the GER fluid.

Next, the radial and vertical shear bands in the axially symmetric profile are analyzed to explain the abundant internal microstructures. We show the radial distribution of particle concentration and shear bands at different heights in Fig. 5 (b). The left-hand column shows the radial distribution of particle concentrations for each lamellar microstructure at different values of h; the red line represents the average concentration. There is a distinct difference in fluctuation for different values of h. The right-hand column shows the radial shear bands of angular velocity distribution at different values of h. The acute position variation of shear bands represents the edge between the particle ring and the oil ring. This can be explained using the classical equation of shear stress and shear rate, $\tau = \eta\dot{\gamma} = \eta\Delta v/\Delta L$. At constant η (viscosity) and ΔL (relative distance between two nearby layers), the shear rate $\dot{\gamma}$ undergoes acute variation when Δv (velocity difference between the two nearby layers) dramatically increases or decreases. This indicates that there is a huge shear stress τ acting on the particle phase, which makes the continuous GER particles phase split into discontinuous phases, which generate particle rings and oil rings. The number and position of particle rings in lamellar microstructures may be determined by the band distribution of radial shearing at certain electric fields. We calculated the distribution of the number density of rings and fluctuation frequency of the radial distribution of shear rate in the inner cell. The dependence of the number density of particle rings on the fluctuation frequency of the radial shear rate is shown in Fig. 6. In the confined disk–disk geometry, high spatial frequency of shear band fluctuation will destroy the formation of particle rings, namely the particle

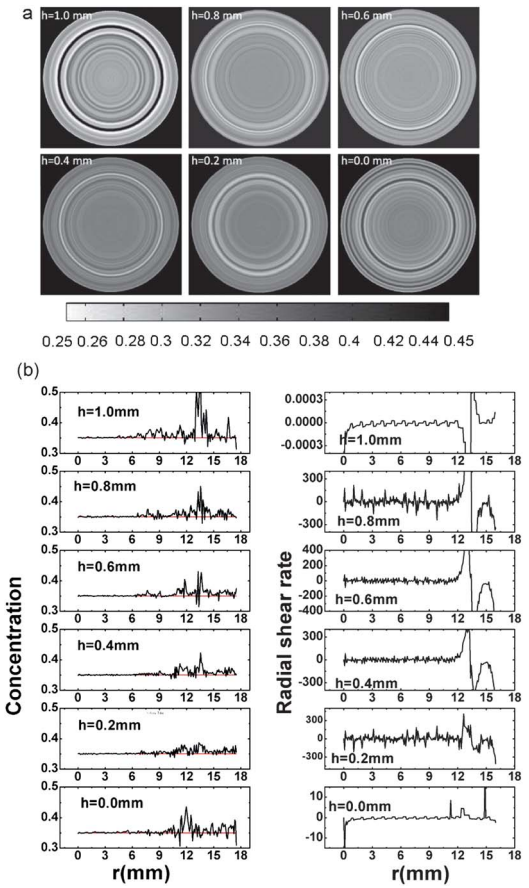

Fig. 5 Internal lamellar microstructures under external conditions of $\dot{\gamma} = 549.5\ s^{-1}$ and $E = 1.3\ kV\ mm^{-1}$ at $t = 20.5$ s. (a) The lamellar microstructure distribution along the electric-field direction from the top ($h = 1.0$ mm) to the bottom ($h = 0.0$ mm) at 0.2 mm intervals. The degree of shading represents particle concentration. (b) The left column is the concentration distribution along the radius r at different values of h. The right column is radial shear rate of angular velocity distribution at different values of h.

structure is thus weakened, which may induce a shear stress reduction. As a result, ring number density decreases with increasing frequency. But when the frequency reaches a certain value, it has less influence on the number density of particle rings.

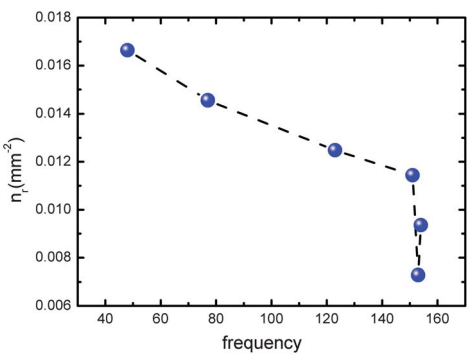

Fig. 6 Dependence of the number density of particle rings on the fluctuation frequency of the radial shear bands in the axial symmetric profile under external conditions of $\dot{\gamma} = 549.5\ s^{-1}$, and $E = 1.3\ kV\ mm^{-1}$ at $t = 20.5$ s.

Next we studied the vertical shear bands parallel to the electric-field direction. Fig. 7 displays changes in shear rate along the sample cell height at different radii of the cell, $r = 1$, 2, 3,…, 16 mm. Both in our experiments (bottom view) and in the simulation, the bottom of the sample cell of the rheological system is steady and the top of the cell is rotating. This geometry gives a nearly zero shear velocity of the fluid close to the bottom, and the highest shear velocity of the fluid close to the top of the cell. In this case, the shear velocity increases from bottom to top, while the shear rate remains constant from bottom to top at a constant radius r. As indicated in Fig. 7, the shear rate increases when the radius increases. Rich distributions of vertical shear bands may cause different lamellar microstructures perpendicular to the electric-field direction. Sharp shear rate changes appear at about $h = 0.1$ and 0.9 mm in the radius region between $r = 7$ and 16 mm. In this area the GER fluids are subject to many different and simultaneous driving and dissipation mechanisms (some of which are not well understood). At high shear rate the laminar flow becomes unstable and there exists a Taylor cell (see Fig.7 (b)). This indicates that there is obvious delamination which represents microstructure weakening. We can draw the conclusion that the rich distribution of vertical shear bands causes different lamellar microstructures perpendicular to the electric-field direction, which may be the origin of shear thinning. Inside the disk–disk sample cell, there exists a competition between the dissipative force, $\eta\dot{S}$, and the electric-interaction conservation force, $-\partial F(S)/\partial S$ (where S is the displacement from equilibrium). The former dominates in the regions away from the rotation axis. So GER particles tend to organize themselves in the shear flow direction, which lowers their viscosity. The particles flow easily around each other at high speed, leading to a lower energy-dissipation rate. The system approaches a balance which is guaranteed by the Onsager principle of minimum energy dissipation rate. Thus, the GER particle concentration tends to fluctuate and form lamellar microstructures governed by the Onsager principle, under both electric interaction and shear flow.

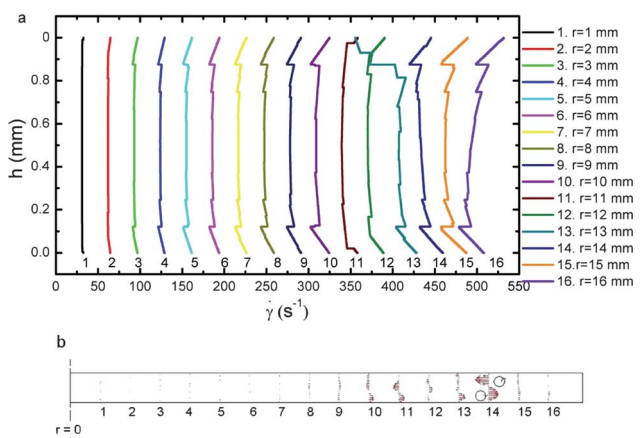

Fig. 7 Colour online. (a) Distribution of internal shear rates along the electric-field direction in the axial symmetric profile under external conditions of $\dot{\gamma} = 549.5\ s^{-1}$ and $E = 1.3\ kV\ mm^{-1}$ at $t = 20.5$ s. The shear velocity is along the $-Z$ axis; see Fig.1 (b). The colors of the lines represent the results for various distances to the rotation axis (r). The drastic change appears at around $h = 0.1$ or 0.9 mm. (b) The red arrow represents the radial velocity profile.

5 Conclusions

We have both experimentally observed surface lamellar microstructures and numerically investigated internal microstructures of shearing GER fluids. By using the two-phase-fluid models, we obtained abundant internal lamellar structures and shear bands in a disk–disk geometry. The numerical results and experiments are in good agreement as far as the ring number density is concerned. Our study shows that the lamellar microstructures are caused by the variation of radial shear bands; and that the vertical shear bands give rise to delamination perpendicular to the flow direction, which lowers their viscosity. The distribution of shear bands in the inner geometry is governed by the balance of free energy and dissipation. In other words, it is the Onsager principle that yields shear bands and lamellar microstructures in shearing GER fluids. The rich internal microstructures of shearing GER fluids should be taken into account in real applications.

Acknowledgements

We thank Ping Sheng, Rongjia Tao, Peng Tan, Wei Bao, and Jie Zheng for their fruitful help and discussions. This work is supported by the National Natural Science Foundation of China under Grant Nos. 10334020, 10974030 and 10574027. J.P.H. acknowledges the financial support by Fok Ying Tung Education Foundation (No. 131008), by Chinese National Key Basic Research Special Fund (No. 2011CB922004), and by the National Natural Science Foundation of China (No. 11075035). J.W.Z acknowledges grant supports from Science & Technology Commission of Shanghai Municipality (No.10PJ1410300) and Shanghai Municipal Education Commission & Shanghai Education Development Foundation (No. 10SG26).

References

1 S. Henley and F. E. Filisko, *Int. J. Mod. Phys. B*, 2002, **16**, 2286–2292.
2 W. J. Wen, X. X. Huang, S. H. Yang, K. Q. Lu and P. Sheng, *Nat. Mater.*, 2003, **2**, 727–730.
3 X. H. Liu, J. J. Guo, Y. C. Cheng, G. J. Xu, Y. Li and P. Cui, *Rheol. Acta*, 2010, **49**, 837–843.
4 J. G. Cao, J. P. Huang and L. W. Zhou, *J. Phys. Chem. B*, 2006, **110**, 11635–11639.
5 Y. Lu, R. Shen, X. Z. Wang, G. Sun and K. Q. Lu, *Smart Mater. Struct.*, 2009, **18**, 025012.
6 R. Tao, *Chem. Eng. Sci.*, 2006, **61**, 2186–2190.
7 D. K. Liu, C. Li, J. Yao, L. W. Zhou and J. P. Huang, *Int. J. Mod. Phys. B*, 2011, **25**, 971–977.
8 W. J. Wen, X. X. Huang and P. Sheng, *Soft Matter*, 2008, **4**, 200.
9 X. P. Zhao and J. B. Yin, *Chem. Mater.*, 2002, **14**, 2258–2263.
10 J. B. Yin and X. P. Zhao, *Chem. Mater.*, 2004, **16**, 321–328.
11 J. W. Zhang, X. Q. Gong, C. Liu, W. J. Wen and P. Sheng, *Phys. Rev. Lett.*, 2008, **101**, 194503.
12 K. von Pfeil, M. D. Graham, D. J. Klingenberg and J. F. Morris, *J. Appl. Phys.*, 2003, **93**, 5769.
13 K. von Pfeil, M. D. Graham, D. J. Klingenberg and J. F. Morris, *Phys. Rev. Lett.*, 2002, **88**, 188301.
14 L. Xu, W. J. Tian, X. F. Wu, J. G. Cao, L. W. Zhou, J. P. Huang and G. Q. Guo, *J. Mater. Res.*, 2008, **23**, 409.
15 X. L. Tang, W. H. Li, X. J. Wang and P. Q. Zhang, *Int. J. Mod. Phys. B*, 1999, **13**, 1806.
16 L. Onsager and S. Machlup, *Phys. Rev.*, 1953, **91**, 1505.

17 M. Doi, *J. Phys.: Condens. Matter*, 2011, **23**, 284118.
18 P. Sheng and W. J. Wen, *Solid State Commun.*, 2010, **150**, 1023.
19 P. Sheng, J. W. Zhang and C. Liu, *Prog. Theor. Phys., Suppl.*, 2008, **175**, 131.
20 K. Q. Lu, R. Shen, X. Z. Wang, G. Sun, W. J. Wen and J. X. Liu, *Chin. Phys.*, 2006, **15**, 2476.
21 P. Tan, W. J. Tian, X. F. Wu, J. Y. Huang, L. W. Zhou and J. P. Huang, *J. Phys. Chem. B*, 2009, **113**, 9092.